4-15-1997

A generalized solidification model and microstructural verification for the Nd–Fe–B–Ti–C system processed by rapid solidification

Matthew J. Kramer
Iowa State University, mjkramer@ameslab.gov

C.P. Li
Iowa State University, Ames, Iowa

K.W. Dennis
Iowa State University, Ames, Iowa

R.W. McCallum
Iowa State University, Ames, Iowa

C.H. Sellers
Lockheed Martin Idaho Technologies, Idaho National Engineering Laboratory, Idaho Falls, Idaho

See next page for additional authors

A generalized solidification model and microstructural verification for the Nd–Fe–B–Ti–C system processed by rapid solidification

M. J. Kramer, C. P. Li, K. W. Dennis, and R. W. McCallum
Ames Laboratory, Iowa State University, Ames, Iowa 50011

C. H. Sellers and D. J. Branagan
Lockheed Martin Idaho Technologies, Idaho National Engineering Laboratory, Idaho Falls, Idaho 83415-2218

J. E. Shield
University of Utah, Salt Lake City, Utah 84112

For the $Nd_2Fe_{14}B$ (2-14-1) compound, the optimal grain size should be smaller than the size of the single domain size of 150 nm. Transition metal carbides (TMC) also reduce the quench rate necessary to achieve the optimal or overquenched condition. This allows inert gas atomization (IGA) to produce viable magnetic materials. In this article we will demonstrate that optimal microstructure for the 2-14-1 can be produced by IGA with the addition of TiC. Moreover, a solidification model will be presented to show (1) how recalescence is a critical feature to the evolution of the microstructure in rapidly solidified materials and (2) the role TMC and other solute phases have on inhibiting grain growth so that lower quench rates can be employed. [S0021-8979(97)95108-2]

I. INTRODUCTION

Alloying $Nd_2Fe_{14}B$ (2-14-1) with compound additions of group IVA, VA, and VIA transition metals along with carbon and/or nitrogen was shown to improve the quenchability of these compounds[1] and inhibit grain growth during subsequent annealing even at temperatures as high as 900 °C.[2] The quintary Nd–Fe–B–Ti–C was found to be an ideal system which satisfied specific criteria based on liquid solubility, nonequilibrium and equilibrium solid solubility and high temperature stability.[2] Thus, a composite microstructure is formed consisting of 2-14-1 grains and TiC precipitates at the grain boundaries. This carbide stabilized microstructure impedes grain growth for extended times (24 h) at high temperatures (900 °C). When Ti and C are dissolved in the liquid melt or supercooled glass the intrinsic properties of these phases are changed. Dissolution into the melt alters solidification which results in many beneficial effects such as an inhibition of nucleation of properitectic iron, a reduction of the cooling rate required to obtain the optimal microstructure and an increase in the glass forming ability. Changes in the intrinsic properties of the glass result in an increase in the crystallization temperature which favorably increases the nucleation rate of the grains during crystallization. Much higher levels of magnetic energy product are obtained after crystallization due to the finer and more uniform grain size.

The changes in quenching characteristics of the liquid melt from simultaneous additions of Ti and C were found to be very applicable to inert gas atomization (IGA). Commercial press/sinter (Sumitomo) and melt-spun (Magnequench) compositions were found to be incompatible with gas atomization.[3] The enhanced quenching characteristics incorporating TiC additions overcomes previous problems in IGA processing of rare earth permanent magnets. Alloys can now be produced in an overquenched condition rather than the underquenched condition of previous alloys. In this article we will compare the evolution of the microstructure in optimally quenched and annealed TiC modified 2-14-1 by IGA to that of optimally quenched 2-14-1 produced by melt-spinning.

II. EXPERIMENTAL TECHNIQUES

A. Inert gas atomization

Five pound charges of commercially pure induction melted ingots were IGA atomized at the INEL using a close coupled nozzle design with an annular gas flow. The atomization processing conditions were optimized to produce a 50% cumulative weight fraction powder size below 20 μm. The processing parameters were similar to those reported previously.[4] The powders were classified by sieving and two size fractions were studied, 10–20 μm and 50–75 μm. Heat treating was done in an inductively heated vacuum furnace (0.1 MPa). The samples were heated from room temperature at a 120 °C min heating rate to the heat treatment temperature, held for 10 min, and then furnace cooled. Due to the low mass of the water cooled furnace, the cooling rate was relatively fast.

B. Melt-spinning

Melt-spinning was performed at the Ames Laboratory by inductively heating an arc-melted ingot in a quartz crucible in an Ar atmosphere to 1350 °C. The melt was ejected through an orifice of 0.8 mm diameter onto a rapidly rotating copper wheel with a 125 Torr over-pressure of Ar. Four separate batches where made with wheel speeds of 10, 20, 30 and 40 m/s.

III. RESULTS

Magnetization measurements of the TiC added melt-spun ribbons showed energy product of 15 MGOe for optimally quenched material. In overquenched samples, the energy product is insensitive to heat treatments above the

crystallization temperature due to grain boundary pinning of the TiC.[2] In the size fraction of <20 μm, the heat-treated GA samples had energy products up to nearly 9 MGOe which dropped to <1 MGOe for powder sizes >50 μm. In addition, the finer size fraction of the GA powders showed an inflection in the second quadrant of the magnetization curve, indicating a bimodal grain size distribution.[5]

Transmission electron microscope (TEM) cross sections of the atomized spheres show a distinct core-rim microstructure regardless of particle size or the post-heat treatment. The outer 60–80 nm consists of fine (10–20 nm), equiaxed grains consisting of 2-14-1 and a much finer grained (5 nm) TiC homogeneously distributed (Fig. 1) in the as-atomized samples. In addition, the surface of the atomized samples and heat treated samples shows irregular shaped grains with a larger size distribution. Auger analysis of these spheres shows that a 15 nm native oxide. The interior of the particles are much coarser grained (80–200 nm) with the interior grains tending to be larger for the larger spheres.

The microstructure across an individual melt-spun ribbon is highly variable from wheel-side to the free-side. For low quench rates (i.e., 10 m/s wheel speed), the wheel side shows first a thin layer ($\sim$0.3 μm) consisting of fine (30–60 nm) equiaxed 2-14-1 grains followed by a thicker region ($\sim$20 μm) where the equiaxed 2-14-1 grains systematically coarsen from $<$100 to 300 nm. In this region, there are frequently α Fe grains at the triple points (Fig. 2). There is yet another transition region where very large 2-14-1 grains (up to 1 μm) have thin layers (50 nm) of α Fe at the grain boundaries. This gives way to a region of very large 2-14-1 grains ($>$10 μm) with aligned α Fe inclusions. The α Fe inclusions have a pinch and swell morphology and are up 30 nm wide (Fig. 3).

For the higher wheel speeds, the grain size at the wheel side get smaller, eventually becoming amorphous. At 20 m/s, a very fine ($<$10 nm) columnar structure of γ Fe is observed at the wheel side. While a full cross section could not be observed in this sample, the middle of the ribbon was fine equiaxed 2-14-1. The free-side again showed very large 2-14-1 with aligned α Fe inclusions as in Fig. 3. At 30 and 40 m/s, the cross section showed very irregular microstructure. The amount of amorphous material increased with the high wheel speeds, but both samples showed pockets of coarsely crystalline material. At higher wheel speeds, the melt-pool on the Cu block is unstable, resulting in pockets along the base of the ribbon which are no longer in contact with the wheel.

IV. DISCUSSION AND CONCLUSIONS

The detailed analysis of melt-spun ribbon and IGA powder shows several unique microstructures which cannot be explained using existing solidification models. These include transition from fine grained equiaxed 2-14-1 to coarse grained 2-14-1 with α Fe dentrites in melt-spun ribbons and the bimodal grain size in IGA powders. We propose a generalized solidification model based upon dentritic breakup during recalesence.[6]

Numerous models have been proposed to the formation of the microstructure in both atomized and melt-spun alloys.[7,8] Most are concerned with competition between free energy of nucleation versus growth. These models have a number of short comings when applied to the 2-14-1 system. Two primary deficiencies are the lack of consideration of peritectic reactions and the failure to account for the effects of the heat of crystallization, i.e., recalescence.

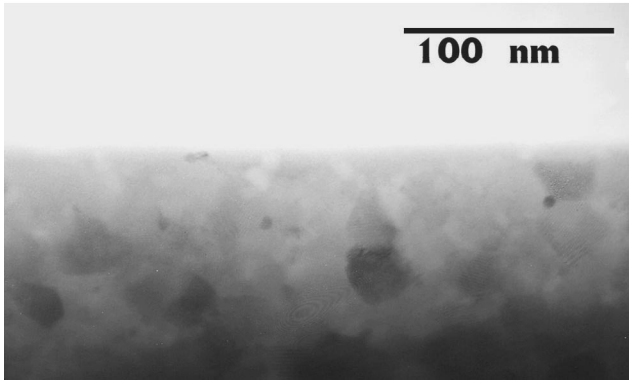

FIG. 1. TEM micrograph of the rim of a GA (10–20 μm) particle showing an equaxed microstructure with fine TiC inclusions.

For the following discussion, we define: T=growth front temperature, T_l=liquidus temperature, T_p=peritectic temperature, T_e=eutectic temperature, T_n=nucleation temperature T_g=glass temperature, T_r=maximum recalescence temperature, α=primary solidification phase, in this case γ Fe, β=peritectic phase, $\beta \rightarrow \alpha$ + liquid at T_p, in this case $Nd_2Fe_{14}B$.

We assume strict directional solidification starting from the wheel surface and no heterogeneous nucleation within the bulk. In this case, the growth front advances in the direction of highest thermal gradient. Starting from an equilibrium condition above T_l, the sample is undercooled to a temperature, T_n, where nucleation occurs. We will restrict our discussion to the case where $T_g < T_n < T_p$. When the β phase nucleates, the solidification front moves very rapidly so that the heat of crystallization exceeds the ability to transfer heat through the solid layer and the interface with the wheel. The temperature of the material and, in particular, the growth front then starts to rise. This is referred to as recalescence. For the case of interest, $T_r > T_p$, so that when T exceeds T_p, the growth of the β phase dendrites is replaced by the growth of α phase dendrites. Recalescence stops when T_r is reached. T_r is determined by the balance of the specific heat of the liquid, the specific heat of the solids, the heat of crystallization of both α and β, the volume fraction of phases the degree of initial undercooling, and the rate of heat extraction to the wheel. Of course T_r may not exceed T_l. After T_r is reached, there is a period where there is a quasistatic plateau, the growth front velocity has slowed to where the heat of crystallization and the heat extracted from the sample are equal. Since the temperature of the material is now above T_p, fine β phase dendrites which formed initially are now unstable and begin to dissolve. At the same time, α phase dendrites are growing at the growth front. Since the material is cooling at a reasonably rapid rate, the temperature soon drops below T_p. At this time, the region of the sample where the primary β phase dendrites have broken up, solidifies rap-

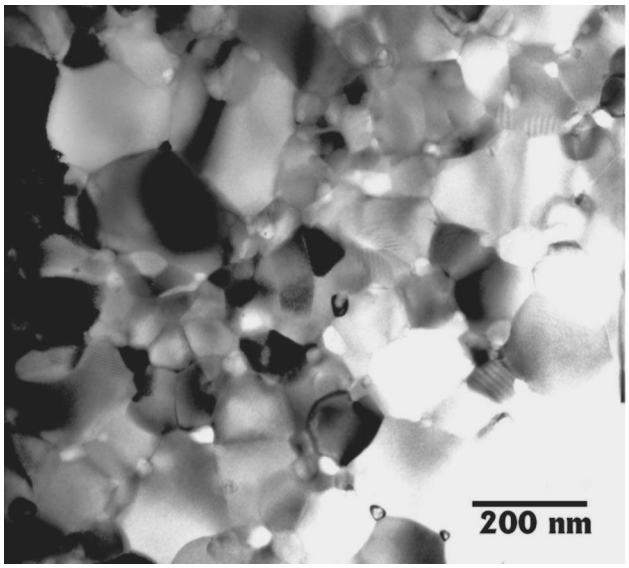

FIG. 2. TEM micrograph of the second layer within the melt-spun ribbon (10 m/s) showing a fine equaxed microstructure of 2-14-1 with α Fe at the triple points.

idly into a fine grained structure nucleated on the dendrite fragments. In the region of the material where α phase dendrites have grown, the composition of the liquid is now such that β phase can nucleate from the liquid. Since homogeneous nucleation is slow, a coarse grained β phase grows around the α phase dendrites which dissolve to some extent. When the material cools below T_e, the microstructural evolution essentially stops.

Using this model, we arrive at a microstructure with two distinct regions. The region which originally solidified with $T < T_p$ exhibits a uniform fine equiaxed β phase structure, while the region which originally solidified with $T > T_p \alpha$ phase has a coarse equiaxed β phase structure with α phase dendrites. Since the change from $T < T_p$ to $T > T_p$ is very distinct, the interface between these two regions will be sharp. In addition, the undissolved α phase dendrites should have a distinct crystallographic orientation. This clearly applies to the majority of conditions of interest and may be applied to Nd–Fe–B to explain the microstructures observed in both the melt spun ribbon and IGA powder. The relative thickness of the layers is highly dependent on solidification parameters and under suitable conditions the bulk of the material may be composed of uniform fine equiaxed β phase structure.

One of the important parameters of this model is the degree of recalescence which occurs. One factor which influences this is the velocity of the growth front which determines the rate at which the heat of crystallization is released. If the velocity of the growth front can be limited, recalescence can be suppressed which explains the remarkable depression of the wheel velocity required to obtain amorphous material by the addition of TiC to Nd–Fe–B. TiC is soluble in the Nd–Fe–B melt up to approximately 6 at. %(3 at.%Ti and 3 at. %C). From the Fe–Ti–C phase diagram, it is clear that the liquidus on the TiC side is steep so that excess TiC produces a saturated liquid with coarse primary TiC precipitates which is consistent with experimental data. TiC is not soluble in the 2-14-1 phase. When the liquid is melt-spun, the solidification front starts at the wheel surface. The undercooling at the surface is sufficient to produce 2-14-1 as the primary phase which results in TiC being rejected to the liquid in front of the interface. This creates a liquid which is supersaturated with TiC in front of the interface so that TiC precipitates out of solution in front of the interface. These particles serve to restrict the motion of the interface. With the interface moving slower, the liquid in front of the interface experiences greater under-cooling and can be cooled below the glass transition temperature without crystallizing. Even if the undercooling is not sufficient to prevent crystallization, the slower velocity of the solidification front reduces the temperature rise due to recalescence since heat is being released at a slower rate relative to the rate at which it is radiated. Thus, it is now possible to optimally quench 2-14-1 using a slower quenching process, such as IGA.

FIG. 3. TEM micrograph of the top layer of the 10 m/s ribbon showing very large 2-14-1 grains with aligned filaments of Fe.

ACKNOWLEDGMENTS

Research at Ames laboratory was funded by USDOE through Iowa State University under Contract No. W-7405-Eng-82. Work at INEL was supported by the DOE Division of Basic Energy Science under DOE Idaho Operations Office Contract No. DE-AC07-94ID13223.

[1] D. J. Branagan and R. W. McCallum, J. Alloys Compd. **218**, 143 (1995).
[2] D. J. Branagan, M. J. Kramer, and R. W. .McCallum, J. Alloys Compd. **244**, 27 (1996).
[3] L. H. Lewis, C. H. Sellers, and V. Panchanathan, IEEE Trans. Magn. **31**, 3641 (1995).
[4] D. J. Branagan, T. A. Hyde, C. H. Sellers, and R. W. McCallum, J. Phys. D (in press).
[5] R. Ramesh, G. Thomas, and B. M. Ma, J. Appl. Phys. **64**, 6416 (1988).
[6] M. Schwarz, A. Karma, K. Eckler, and D. M. Herlach, Phys. Rev. Lett. **73**, 1380 (1994).
[7] B. X. Gu, H. R. Zhai, and B. G. Shen, J. Magn. Magn. Mater. **97**, 40 (1991).
[8] K. H. J. Buschow, D. B. DeMooji, and H. M. Van Noort, J. Less-Common Met. **125**, 135 (1986).